Chapter 5

Electrochemical detection of antimalarial drug Primaquine based on MoS_2 nanosheets - gold nanorods nanocomposite modified electrode

5.1 General Introduction

Malaria is one of the most common life-threatening infectious diseases prevalent in the tropical and subtropical regions of the globe, and it is a global public health challenge. It has resulted in billions of deaths in the last decade. The disease is a parasitic disease caused by unicellular protozoans of the Plasmodium group and transmitted to the human through a vector named female Anopheles mosquito [WHO, World Malaria Report 2018; WHO, 2019]. Primaquine (PQ), chemically called N-(6-methoxyquinolin-8-yl) pentane-1,4-diamine, is a commonly used anti-malarial drug that has been prescribed by World Health Organization (WHO) for the medication against the lethal infections caused by *Plasmodium vivax* and *Plasmodium ovale* [Fernando, 2011]. Its mechanism of action also reduces the risk of transmission in case of infection from *P. falciparum* [Clyde, 1981]. The drug is also used for the treatment of Pneumocystis infections which is a serious source of pneumonia in HIV-infected patients with weakened immune systems [Fishman, 1998; Thomas and Limper, 2004; Thomas and Limper, 2007].

Clinical investigations apprised that PQ has a very narrow therapeutic window and shows peculiar side effects hence PQ is prescribed to a patient with intense care [Arguin and Tan, 2016]. There are some adverse side effects such as hemolytic anemia in patients with Glucose-6-phosphate (G6P) deficiency, gastrointestinal disturbance and methemoglobinemia. Other common side effects include headache, cardiac arrhythmia, leucopenia, hypertension, etc. [Beutler, 1990; Galappaththy et al., 2013; Martins et al., 2015]. Studies indicate that the PQ is unstable photo-chemically and the toxicity of the

drug may be attributed to some photo-derivatives [Kristensen, 1993]. Because of these factors, the applicability of this drug is limited. Therefore, the analytical estimation of PQ in real samples is of utmost importance.

Various techniques have been employed in the past for the quantitative estimation of PQ such as spectrophotometry [Karad and Barhate, 2015], colorimetry [John, 1996], fluorimetry [Tsuchiya et al., 1984], HPLC [Dwivedi et al., 2003; Miranda et al., 2015] and mass spectrometry [Bangchang et al., 2014]. These technologies might give a good sensitivity, but they are costly, tedious, require long analysis time, sophisticated instrumentation, and need a skilled operator. In contrast to these techniques, the electrochemical methods bear a range of advantages such as robustness, rapidness, simplicity and high sensitivity with easier instrumentation that make them the most acceptable candidate for drug sensing. Very few reports have been published for electrochemical quantification of PQ [Mashhadizadeh and Akbarian, 2009; Arguelho et al., 2005; Thapliyal et al., 2017; Prasad et al., 2016; Marlin et al., 2019]. In Table 5.5, a list of electro-analytical reports has been presented with a comparison of their efficacy and merits.

TMDs are an important class of layered 2D nanomaterials and recently gathered growing attention in many applications due to their fascinating chemical, physical and electronic properties. Among various TMDs, MoS_2 has grabbed more attention due to its properties better than other TMDs [Zhang et al., 2016; Laursen et al., 2012; Daniloska et al, 2010; Upadhyay et al., 2016; Sun et al., 2013]. MoS_2 nanosheet has a single-layered nanostructure and has immense potential to behave as a graphene analogue. It is comprised of atomic layers of S-Mo-S rendering it a sandwich-like structure wherein the hexagonal plane of Mo is sandwiched between the planes of S

atoms and these three layers are adhered to one another by weak van der Waals forces [Chang and Chen, 2011]. The layered nanostructure of MoS_2 provides a large surface area, great thermal conductivity and electrical conductivity, and remarkable charge carrier mobility to the material. These properties make it a magnificent candidate to be utilized for promising applications such as catalysis, sensors, electronics, optoelectronics and energy storage.

However, it is not an immediately selected electrode material since it has a semi-insulating behaviour. Further, another challenge faced while using chemically exfoliated nanosheet is that it has a tendency for restacking during processing while experimentation, thereby reducing the number of active sites and hence deteriorating the desired charge transport properties. The surface modification of MoS_2 nanosheets can improvise the dispersion, processability and charge transport properties to exploit its unique nanostructures more efficiently. Conducting polymers, carbonaceous materials and metal nanoparticles are mostly used for tuning the characteristics of MoS_2 nanosheets [Wang et al., 2013; Li and Du, 2017; Saraf et al., 2018].

Metal nanoparticles, for instance, gold and silver, are used as spacers between the different layers of MoS_2 nanosheets and check restacking [Solanki, 2018]. Au NPs are attractive and most preferred since they exhibit a high extent of structural connectivity throughout the surface, high specific surface area and catalytic properties. Such properties make them a potential candidate for applications in sensing, catalysis, optoelectronics, etc. Various shapes such as spherical, rods, etc. can be obtained depending upon the reducing agent, reaction conditions, reactions time, pH, etc., and properties and potential applications can be tuned [López-Lorente, 2021; Hong et al., 2015]. GNR are long rod-like structures with characteristic electronic and optical

properties depending upon their dimension. GNR have showcased their potential applications in the field of biomedicine, imaging, and sensing [Solanki et al., 2018; Ojha et al., 2022; Jayabal et al., 2014]. A significant difficulty that is faced while using metal nanoparticles in sensing applications is their rapid aggregation behaviour, i.e. quite low stability. In order to get rid of this problem, a large number of materials are utilized as a support, such as CNT [Pang et al, 2009], GO [Ensafi et al, 2015], rGO [Jayabal et al., 2014] and graphitic C_3N_4 [Ojha et al., 2022], etc. Inspired by the commendable properties of MoS_2 nanosheet and GNR, as well as keeping in view the shortcomings of both the species individually, we herein have fabricated a composite out of the two components. Due to the synergistic effect, the shortcomings of the two individual components have been eliminated, and the performance of the synthesized nanomaterial has been enhanced.

In the current study, we have developed MoS_2 nanosheets via a single-step hydrothermal synthesis with controlled morphology. We have also synthesized uniformly sized GNR through a seed-mediated approach. The MoS_2 nanosheets were firstly exfoliated in water followed by ultrasonication in the presence of GNR to fabricate a nanocomposite of MoS_2 nanosheets and GNR (MoS_2-GNR). The ratio of the components has also been optimized for the best performance. The resulting composite was characterized by FTIR, XRD, TEM, CV and EIS. Further, the as-synthesized composite has displayed exceptional electroactive properties and has been exploited as an electron nanomediator for the electrochemical sensing of an antimalarial drug PQ through DPV. The performance of the developed sensor has also been validated in complex real samples like human blood serum and pharmaceutical preparation.

5.2 Experimental Section

5.2.1 Chemicals and Materials

PQ was procured from Sigma Aldrich, India and used without further purification. Gold chloride trihydrate ($HAuCl_4 \cdot 3H_2O$) was obtained from Sisco Research Laboratories Pvt. Ltd, India (SRL Chemical). Sodium molybdate dihydrate ($Na_2MoO_4.2H_2O$), L-Cysteine ($HO_2CCH(NH_2)CH_2SH$), sodium dihydrogen phosphate (NaH_2PO_4), conc. HCl, disodium hydrogen phosphate (Na_2HPO_4), $AgNO_3$, AA and all other chemicals were procured from Merck (Merck India). The buffer solutions were prepared by mixing 0.1 M NaH_2PO_4 and Na_2HPO_4 solutions. DI water was utilized in all the preparations and experimentations. Blood samples were collected from Sir Sunder Lal Hospital, BHU, Varanasi for the quantitative estimation of PQ in human blood serum. PQ tablets were purchased from a common drugstore.

5.2.2 Synthesis of MoS_2 nanosheets

For the synthesis of MoS_2 nanosheets, a facile one-step hydrothermal route was adopted which is described previously by our lab group and represented in Figure 5.1 [Mall et al., 2022]. For instance, 250 mg sodium molybdate dihydrate, and 500 mg Cysteine (1:2 w/w) were added in different beakers having 25 mL DI water, and stirred constantly for half an hour. These two solutions were mixed together and continuously stirred for around 30 min, while maintaining the temperature at ~40 ℃ and pH at 3.0. Conc. HCl was employed to maintain the acidic pH. The resulting mixture was transferred into the stainless steel-lined Teflon autoclave and constantly maintained at ~200 ℃ for 40 h. Then, the obtained solution was naturally allowed to cool down to RT leaving behind a dark brown product. This precipitate was centrifuged at 6000 rpm and appropriately

washed with water, followed by ethanol. At last, it was vaccum dried at ~70 °C overnight. A plausible mechanism for the synthesis of MoS_2 nanosheets has already been presented in previous chapter.

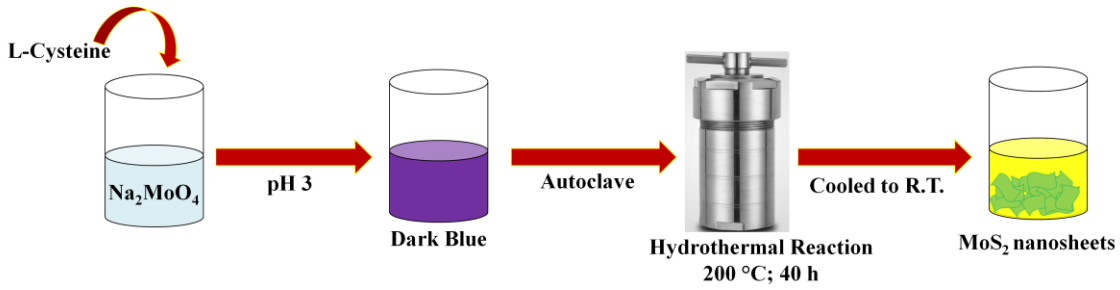

Figure 5.1 Hydrothermal synthesis of MoS_2 nanosheets

5.2.3 Synthesis of GNR

In our study, we have opted for a seed-mediated growth methodology for the preparation of GNR reported by Ojha et al. and shown in Figure 5.2 [Ojha et al., 2022]. First step is the preparation of seed solution. 5 mL $HAuCl_4$ solution (0.5 mM) was dropwise mixed into 5 mL CTAB solution (0.2 M) with stirring. The colour of the solution becomes light yellow and stirring continued for 1 h. Then, a mixture of 600 µL $NaBH_4$ solution (0.01 M) and 40 µL DI water was added in one slot to the above-mentioned reaction mixture with vigorous stirring (2000 rpm). The colour of the mixture turned brownish yellow and stirring was ceased immediately after 2 min, then the mixture was kept undisturbed for 30 min at RT. Further, a growth solution was prepared separately in the second step. 5 mL 0.2 M CTAB suspension was prepared and heated around 50-70 °C to completely dissolve CTAB, followed by cooling to RT. Then, 150 µL 0.004 M $AgNO_3$ solution was added and the resulting mixture was then kept interrupted for 15 min at 30 °C. Then, 5 mL $HAuCl_4$ (1 mM) solution was dropwise added to the reaction mixture with stirring, and stirring continued for 15 min.

Now, 70 µL AA (78.8 mM) was further mixed into the reaction mixture followed by stirring at high speed until the colour of the mixture disappeared. Finally, 12 µL of the previously prepared seed solution was added to the reaction mixture with continuous stirring for 30 s. Now, the final solution was kept undisturbed for 24 h at 30 °C for elongated growth of GNR. Finally, the light violet coloured uniform GNR solution was achieved which was centrifuged at 10000 rpm to remove the excess CTAB present in the solution. Now, 10 mL of DI water was mixed with the precipitate to yield the final GNR solution which was further used in all the experiments.

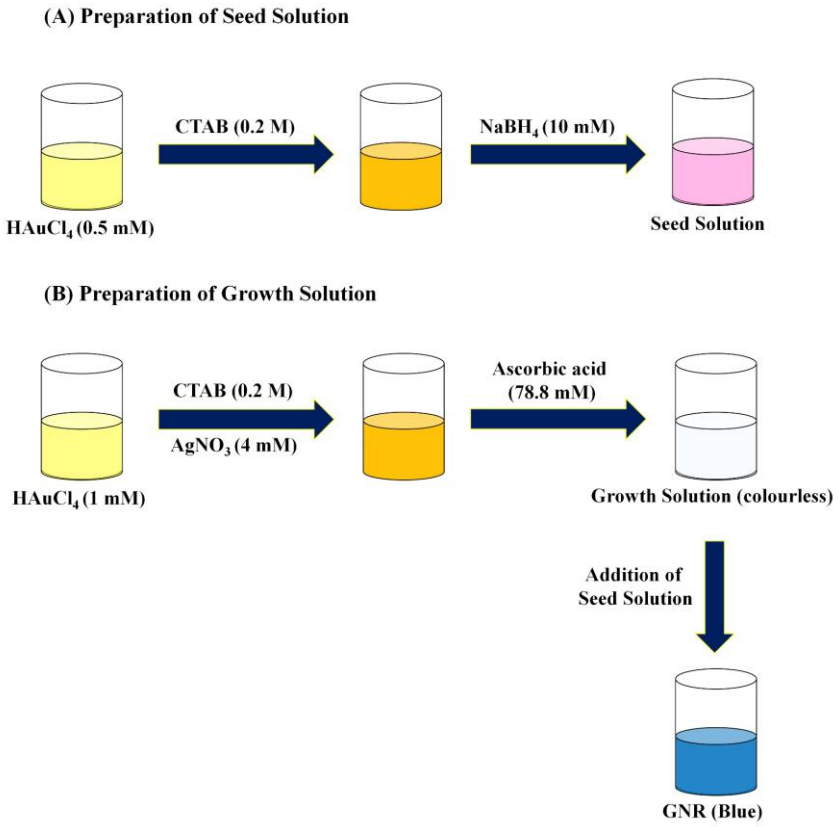

Figure 5.2 Preparation of GNR by seed-mediated growth methodology

A widely adopted chemical reaction occurring during the seed mediated growth methodology for the growth of GNR can be expressed as follows;

$$2HAuCl_4 + 3C_6H_8O_6 \xrightarrow[Au^0\ (nanosphere)]{CTAB,\ Ag^+} 2Au^0\ (nanorod) + 3C_6H_6O_6 + 8HCl \quad \text{(Eq. 5.1)}$$

where $C_6H_8O_6$ denotes ascorbic acid which is oxidised to $C_6H_6O_6$ (dehydroascorbic acid). The addition $AgNO_3$ helps to provide the shape control.

During the seed mediated growth, GNR are synthesized by the introduction of small gold nanoparticle seeds (through the seed solution) to the growth solution containing a mixture of CTAB (surfactant), gold ions ($AuCl_4^-$), a weak reducing agent (AA), and silver ions. The dimensions of the resultant GNR are typically regulated by the amount of Au NP seeds and/or by the silver ion concentration.

5.2.4 Synthesis of MoS_2-GNR composite

Figure 5.3 showcases the synthesis of the MoS_2-GNR composite. Initially, 5 mg MoS_2 nanosheet was exfoliated by dispersing in 5 mL DI followed by ultrasonication for 1 h. 500 μL prepared GNR solution was introduced into the MoS_2 suspension and it was again ultrasonicated for 2 h. The resulting mixture was centrifuged at 8000 rpm and properly washed with DI water, followed by ethanol. Finally, the precipitate was dried in a vaccum oven at 60 °C to yield the final composite MoS_2-GNR. Similarly, seven sets of composites were synthesized by varying the amount of GNR (500 μL, 2500 μL, 3500 μL, 5 mL and 15 mL), and named 1:1, 1:5, 1:7, 1:10 and 1:30 respectively.

Figure 5.3 Schematic pathway for the synthesis of MoS_2-GNR nanocomposite

5.3 Results and Discussions

5.3.1 Structural Analysis

The structural investigation of synthesized nanocomposite has been performed by XRD technique, FTIR spectroscopy and TEM. Figure 5.4 (a) demonstrates the XRD pattern of MoS_2 nanosheet, GNR and MoS_2-GNR nanocomposite. The diffraction pattern of MoS_2 nanosheet indicates the signals at 2θ = 10°, 32°, 43° and 57° corresponding to planes (002), (100), (103) and (110) respectively which show the hexagonal plane of MoS_2 nanosheet (JSPDS 37-1492) [Mishra et al., 2017]. In the XRD pattern of GNR, four signals were observed positioned at 39°, 45°, 65° and 78° which correspond to (111), (200), (220) and (311) planes of gold respectively [Ojha et al., 2022]. In the case of XRD pattern of the nanocomposite, all the signals of the MoS_2 nanosheet as well as GNR were observed which provide the supporting proof of the incorporation of GNR over the surface of the MoS_2 nanosheet.

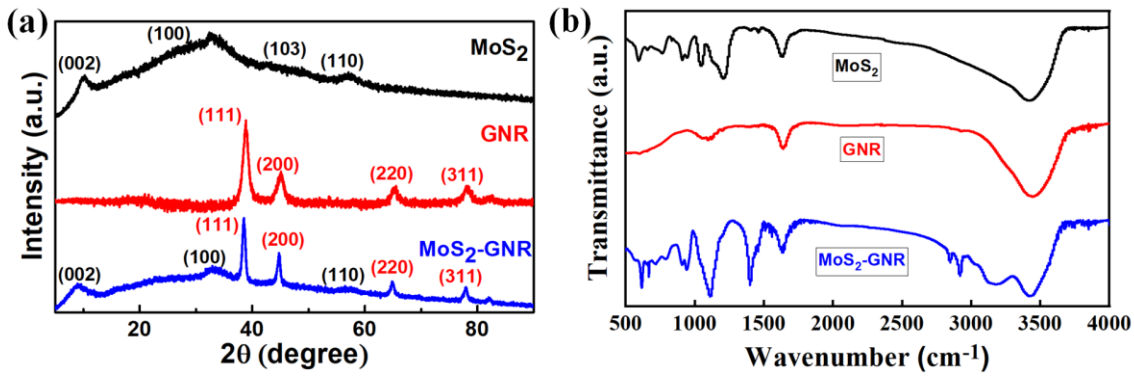

Figure 5.4 (a) XRD spectra, (b) FTIR spectra of MoS_2, GNR and MoS_2-GNR

The functional group analysis and interaction study of MoS_2 nanosheet and GNR were investigated using FTIR spectroscopy. Figure 5.4 (b) expresses the FTIR spectra of the MoS_2 nanosheet, GNR and composite. The FTIR spectra of MoS_2 showed a broad band at 3446 cm^{-1} which was assigned to the OH stretching vibration of adsorbed water

molecules while a peak at 1640 cm^{-1} may be designated to OH bending vibration. For the case of GNR, the FTIR spectrum displayed a broad band at 3432 cm^{-1} due to OH stretching of the adsorbed water while the peak obtained at 1640 cm^{-1} can be attributed to the bending vibration of H_2O. Moreover, the several peaks near 3000 cm^{-1} signify CH stretching, and the band at 1117 cm^{-1} is ascribed to the CN stretching of CTAB. The FTIR results of GNR suggest the conjugation of CTAB onto the surface of GNR. Most substantially, the characteristic FTIR peaks of GNR and MoS_2 were distinguished in the FTIR spectrum of MoS_2-GNR, signifying the loading of GNR on MoS_2. The peaks of CTAB molecules are less prominent in composite due to repeated washing during synthesis steps [Yougbaré et al., 2021; Singh et al., 2021].

TEM micrographs of MoS_2 nanosheet, GNR and MoS_2-GNR composite are shown in Figure 5.5 (a) to (c) to define the internal nature of the materials. Figure 5.5 (a) shows the well-defined sheet-like structure of MoS_2. The elongated rod-shaped GNR can be observed in Figure 5.5 (b). In case of the nanocomposite (Figure 5.5 (c)), it can be seen that the GNR are uniformly distributed on the surface and within the MoS_2 nanosheet. Also, the GNR are very well anchored onto the MoS_2 nanosheet. The SAED pattern of the composite can be seen in Figure 5.5 (f) which contains the ring patterns attributed to the (111) plane of the GNR. It indicates the partly crystalline nature of the composite.

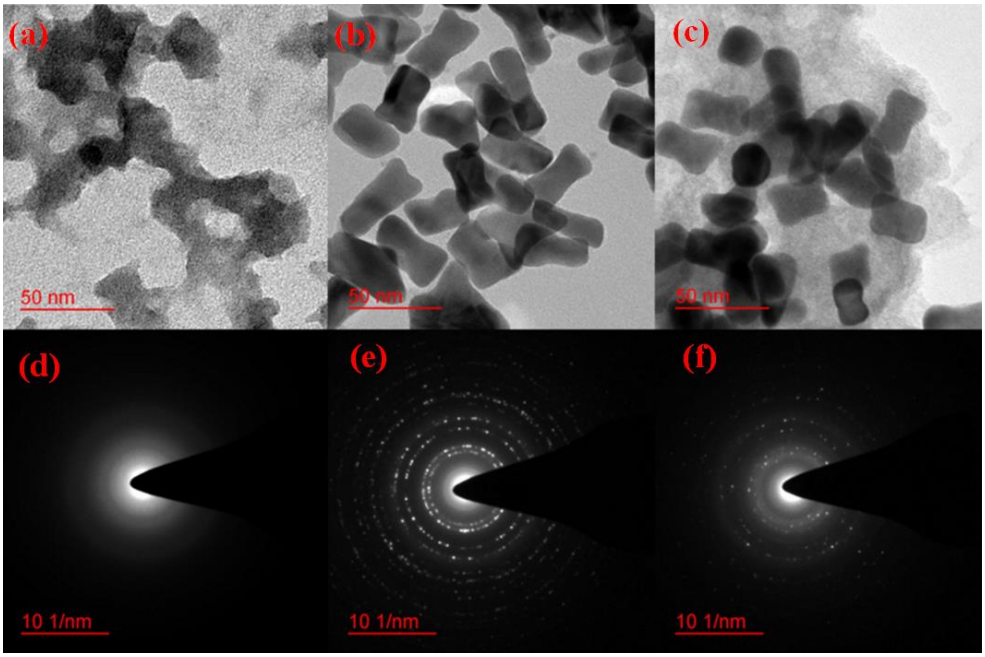

Figure 5.5 TEM micrograph of (a) MoS_2, (b) GNR and (c) MoS_2-GNR, and SAED pattern of (d) MoS_2, (e) GNR and (f) MoS_2-GNR

The elemental composition was investigated by performing XPS characterization of the synthesized MoS_2-GNR. In Figure 5.6 (a), the XPS survey spectrum shows the peaks corresponding to different elements present in the composite. The spectrum shows the existence of Au in a zero oxidation state in addition to Mo and S in the synthesized material signifying the successful anchoring of GNR on the surface of MoS_2. Further, the detailed study was done using the high-resolution deconvoluted XPS spectra. Figure 5.6 (b) exhibits two prominent peaks at 228.4 eV and 232.4 eV attributed to the Mo $3d_{5/2}$ and Mo $3d_{3/2}$ orbital respectively, demonstrating the dominance of Mo^{4+} in the composites [Chen et al., 2011; Ali et al., 2019]. The other peaks corresponding to the +5 and +6 oxidation states may be due to the oxidation of the product during the hydrothermal synthesis. Besides, the peak at 226 eV may be attributed to S 2s [Singh et al., 2021]. In Figure 5.6 (c), the two peaks assigned to S $2p_{3/2}$ and S $2p_{1/2}$ are positioned at 161.3 eV and 162.5 eV respectively, and the $2p_{3/2}$ peak displays a single doublet which is in accordance with the −2 oxidation state of S [Wang et al., 2017]. The

chemical coordination of MoS_2-GNR could be validated using peaks of Mo^{4+} and S^{2-} ions. In Figure 5.6 (d), the signals at 83.7 eV and 87.4 eV correspond to Au $4f_{7/2}$ and Au $4f_{5/2}$ respectively supporting the decoration of GNR on the MoS_2 [Ali et al., 2019].

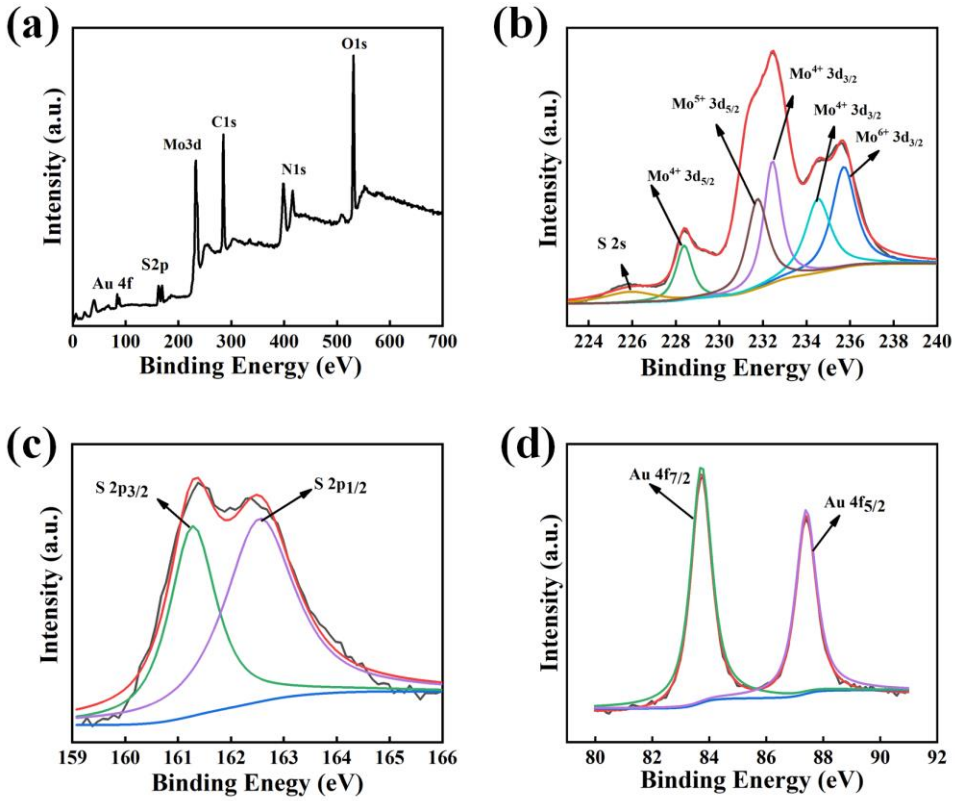

Figure 5.6 XPS characterization (a) XPS survey spectrum, the deconvoluted spectrum of Mo 3d (b), S 2p (c), and Au 4f (d) regions of MoS_2-GNR.

5.3.2 Optimization of the ratio of MoS_2 nanosheet and GNR, and comparison of electroactivity of different prepared electrodes

For the comparison of the electroactivity of the synthesized materials, CV and EIS measurements were recorded for different modified electrodes in 0.1 M PBS containing 5 mM $[Fe(CN)_6]^{3-/4-}$ since this complex is extensively used as a redox probe in electrochemical studies and it exhibits a distinct redox property [Kakaei, 2013]. Figure 5.7 (a) depicts the CV curves of the samples 1:1, 1:5, 1:7, 1:10 and 1:30. It clearly

indicates that with increasing the amount of GNR in the developed composite, the current in CV increases with a reduction in the peak difference between the oxidation and reduction potentials of $[Fe(CN)_6]^{3-/4-}$ signifying better electroactivity of the modified electrode. Figure 5.7 (b) displays the Nyquist Plot of the impedance measurement of aforesaid developed samples of MoS_2-GNR composite. The data reveals that the 1:30 sample possesses the least impedance among the different combinations of the composite. Table 5.1 expresses the potential difference (ΔE) between the oxidation and reduction potential along with anodic and cathodic peak current in the CV, and the R_{ct} value from the Nyquist plots of different MoS_2-GNR samples. The results revealed that the least ΔE value corresponds to the 1:30 sample and the redox peak current was found to be maximum in the case of the 1:30 sample. So, the best electrode performance was observed for the 1:30 sample and hence the amount of GNR was optimized in the composite for the best electroactive performance. Further, 1:30 sample of the composite was finalized for further analyses. For the next description, MoS_2-GNR refers to the 1:30 sample composite.

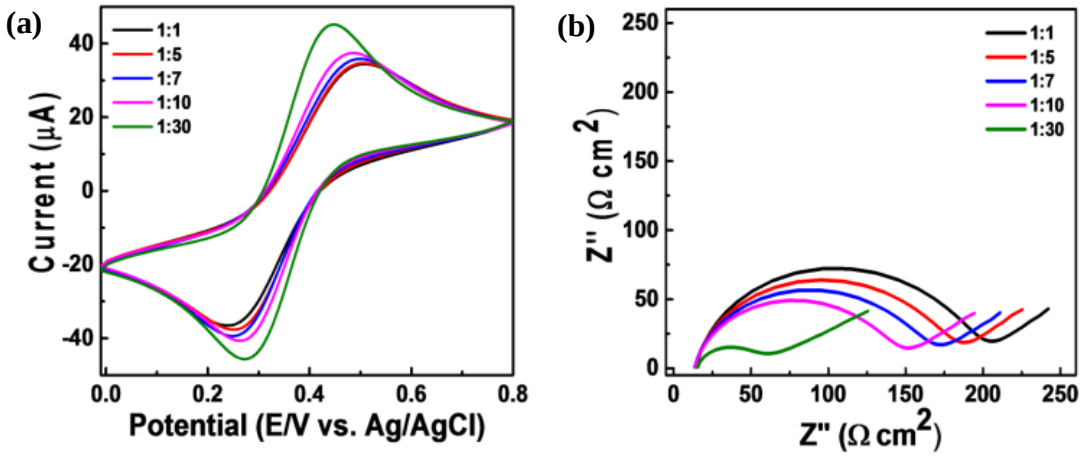

Figure 5.7 Cyclic voltammograms (a) and Nyquist plots (b) of composite samples 1:1, 1:5, 1:7, 1:10, and 1:30 in 5 mM $[Fe(CN)_6]^{3-/4-}$ solution in 0.1 M PBS (pH 7.4)

Table 5.1 Comparison of values of R_{ct} in Nyquist plot and potential difference in CV redox peaks in 5 mM Ferri/Ferro solution in 0.1 M PBS regarding different samples of MoS_2- GNR

Electrode Materials	R_{ct} Value (Ωcm^2)	Redox potential difference ΔE (V)	Oxidation Peak Current Ipa (μA)	Reduction Peak Current Ipc (μA)
1:1	180.40	0.27	34.45	-36.59
1:5	164.30	0.25	34.77	-37.73
1:7	150.20	0.25	35.91	-39.45
1:10	130.70	0.22	37.44	-40.75
1:30	50.73	0.18	45.20	-45.70

5.3.3 Electrochemical characterization of MoS_2-GNR

Now, the performance of bare GCE, MoS_2, GNR, and MoS_2-GNR (1:30) was compared with the help of CV and impedance measurements. Figure 5.8 (a) showcased the CV curves at 20 mV of the synthesized materials. Figure 5.8 (b) shows the Nyquist plot of the impedance measurement of the synthesized electrode materials. Further, based on the results obtained in CV and impedance measurement, Table 5.2 was prepared to feature the ΔE, anodic and cathodic peak current intensity and R_{ct} value from the electrode materials. From Table 5.2, it can be observed that the bare GCE displayed a small R_{ct} value of 40.42 Ωcm^2 and a redox potential difference of 0.14 V. Upon modification with MoS_2, the R_{ct} value increases to 231.7 Ωcm^2 and the redox potential also increases (0.29 V) with a decrease in CV current. This might be due to hindered electron transfer from $[Fe(CN)_6]^{3-/4-}$ to the surface of the electrode because of the poor conductivity of MoS_2 and a large number of negative charges on its surface [Su et al.,

2016; Wu et al., 2012]. The R_{ct} value of MoS_2-GNR was found to be smaller than MoS_2 with the improved current response and reduced redox potential difference signifying better electrochemical properties than pristine MoS_2.

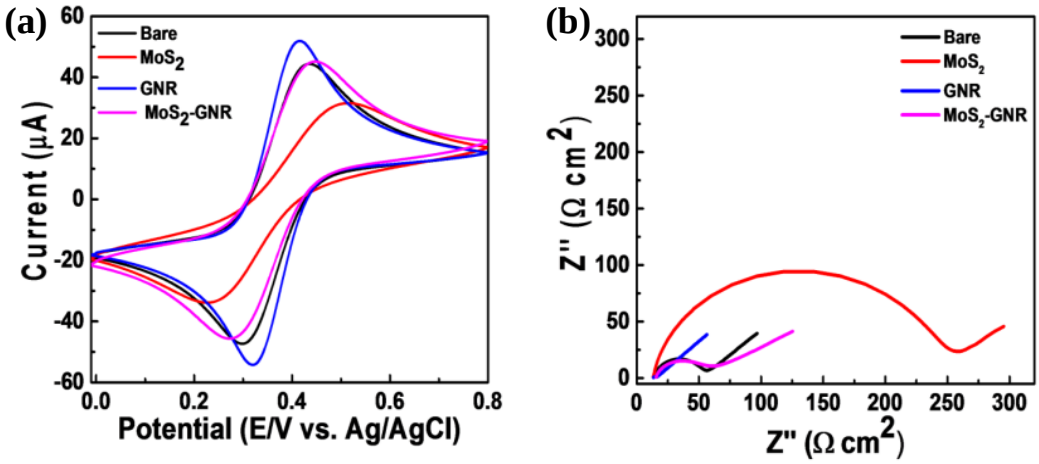

Figure 5.8 Cyclic voltammograms (a) and Nyquist plots (b) of bare GCE, MoS_2, GNR, and MoS_2-GNR composite of 5 mM $[Fe(CN)_6]^{3-/4-}$ in 0.1 M PBS (pH 7.4).

Table 5.2 Comparison of values of R_{ct} in Nyquist Plot, the potential difference in CV redox peaks, and oxidation and reduction peak currents in 5mM Ferri/Ferro solution in 0.1 M PBS regarding different prepared electrode materials.

Electrode Materials	R_{ct} Value (Ωcm^2)	Redox potential difference (V)	Oxidation Peak Current Ipa (µA)	Reduction Peak Current Ipc (µA)
Bare	40.42	0.14	44.38	-47.30
MoS_2	231.70	0.29	31.57	-33.83
GNR	4.36	0.09	51.91	-54.29
MoS_2-GNR	50.73	0.18	45.20	-45.70

5.3.4 Electrochemical sensing of PQ

5.3.4.1 Electrode fabrication

First of all, the GCE was polished on 0.3 µm alumina slurry for cleaning it properly. Then, it was sonicated for 2 min in DI water as well as acetone. A suspension of the MoS_2-GNR composite was prepared by dispersing its 1 mg amount in 1 mL DI water. It was sonicated for around 1 h to result in a homogenous suspension which was drop cast (5µL) onto the disc of the GCE which was dried in a vacuum desiccator for 30 min. Since the prepared composite was insoluble in water, the problem of material leaching from the electrode surface was eliminated.

5.3.4.2 Electrochemical study of PQ at MoS_2-GNR/GCE

The electrochemical investigation of the behavior of PQ was performed by employing CV in 0.1 M PBS (pH 7.4) in the presence of 50 µM PQ at a scan rate of 50 mV/s (Figure 5.9 (a)). The potential window was selected as 0.3 V - 1.1 V and an oxidation peak was perceived at ~0.88 V on a bare GCE with the absence of any peak in the reverse scan. As compared to bare GCE, a current enhancement was obtained at ~0.92 V on MoS_2-GNR/GCE. The current enhancement was attributed to the facilitation of electro-oxidation of PQ at the modified electrode. Figure 5.9 (b) is the Nyquist plot of bare GCE and MoS_2-GNR modified GCE in the presence of PQ (50 µM) in 0.1 M PBS of pH 7.4. The result suggests that the composite has a lower R_{ct} value that facilitates the electron transfer by reducing the interfacial charge transfer resistance. It is presumed that electrocatalytic activity was enhanced by the functionalization of MoS_2 nanosheet by the anchorage of GNR. The resulting nanocomposite exhibited a large surface area and high electrical conductivity providing a large number of active sites which accelerate the transfer of electron at electrode surface. Notably, the electro oxidation of

PQ is obtained due to the involvement of Nitrogen of the quinoline ring, because oxidation of Nitrogen of aliphatic amine requires higher positive potential.

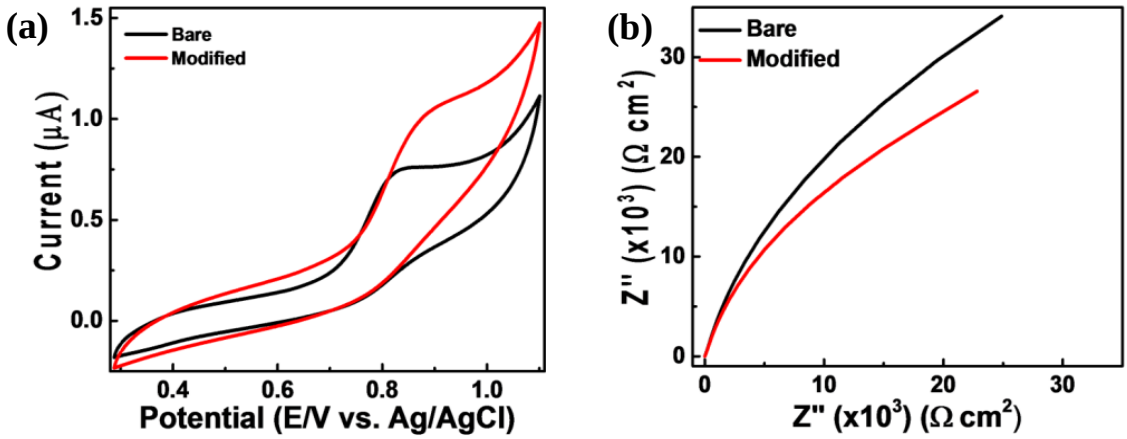

Figure 5.9 (a) CV and (b) Nyquist plots of PQ (50 µM) in 0.1 M PBS of pH 7.4 at bare GCE and MoS_2-GNR modified GCE

5.3.4.3 Optimization of pH of the supporting electrolyte

pH plays a very significant role in the electrochemical sensing of PQ. It has an immense influence on the electrochemical oxidation of PQ. Oxidation of 50 µM PQ was investigated in 0.1 M PBS within the pH range from 5.0 to 10.0 employing CV and DPV techniques. As reported in the previous literature [Ullah et al., 2015], there are two acid-base equilibria involved in PQ oxidation which are as follows: -

1. $PQH_2^+ \rightleftharpoons PQH^+ + H^+$ (Eq. 5.2)

   Diprotonated Monoprotonated

   It is observed at pH ≤ 5.0

2. $PQH^+ \rightleftharpoons PQ + H^+$ (Eq. 5.3)

   Monoprotonated Molecular form

   It is observed at pH ≥ 8.7

The two equilibria clearly indicate the role of H^+ in electrode reaction. Figure 5.10 (a) and (b) represent the CV and DPV curves regarding the pH optimization study. pH 5.0, 6.0, 7.0, 7.4, 9.0 and 10.0 were chosen in our study, and responses were recorded. The obtained results are in agreement with the previous reports and Equations 5.1 and 5.2. The oxidation potential has a higher value at acidic pH and a lower value at alkaline pH. The sharpest response and the maximum current were perceived at pH 7.4 in the case of both CV and DPV. Since pH 7.4 is also the physiological pH of human blood, it was selected for further analytical experiments.

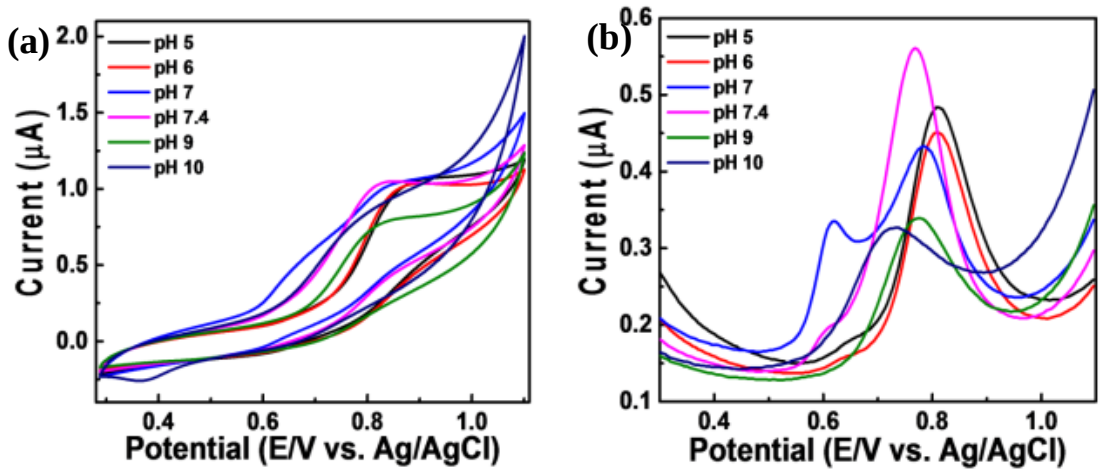

Figure 5.10 (a) CV and (b) DPV of PQ (50 µM) in 0.1 M PBS on MoS_2-GNR modified GCE at pH 5.0, 6.0, 7.0, 7.4, 9.0, and 10.0.

5.3.4.4 Quantitative Estimation of PQ

After optimizing various external parameters described above, the voltammetric experiments were conducted over MoS_2-GNR modified GCE for quantitative estimation of PQ using DPV. DPV parameters such as the potential window from 0.3 V to 1.1 V, step potential of 5 mV, modulation amplitude of 25 mV, modulation time of 50 ms, and interval time of 500 ms were chosen to obtain the best signal. DPV response of the electrode was recorded in PBS (pH 7.4) as a supporting electrolyte with successive addition of PQ in the test solution (shown in Figure 5.11 (a)). The resulting voltammograms illustrate that the anodic peak current enhances with an increment in the concentration of PQ. Figure 5.11 (b) displays a calibration plot between the current and the amount of PQ in the concentration range from 1 µM to 150 µM. Figure 5.11 (b) inset shows that the relationship between current density and the amount of PQ. The curve was found to be linear and this linearity was obtained within the concentration range of 1-82.4 µM. The corresponding regression equation was calculated as Ipa (PQ) = 0.01062C + 0.16167 and correlation coefficient R^2 as 0.99. The LoD was computed

using the formula 3σ/m where σ denotes the relative standard deviation of the blank test solution and m represents the slope of the above-described calibration plot. So, the value of LoD and sensitivity of the MoS_2-GNR modified electrode for PQ detection was measured as 90.2 nM and 0.1517 $\mu A \mu M^{-1} cm^{-2}$ respectively.

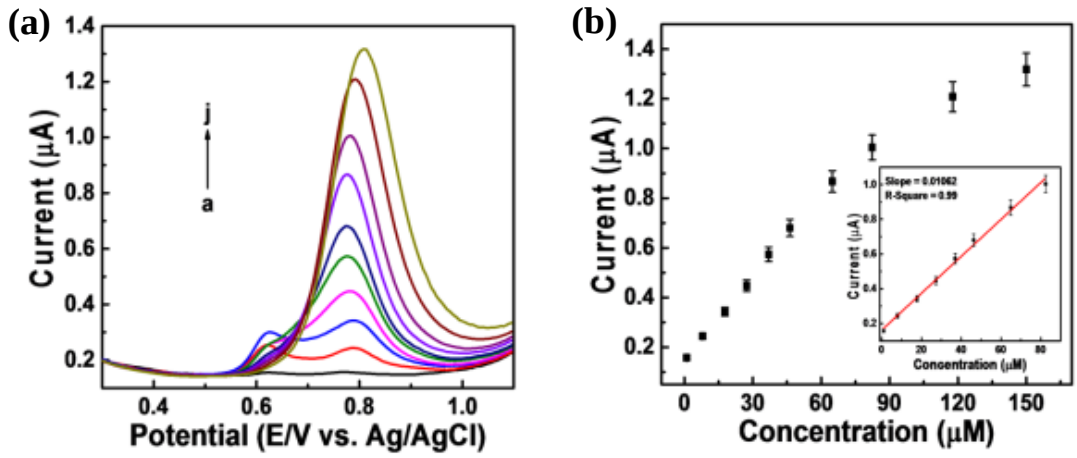

Figure 5.11 (a) DPV measurements and (b) linear calibration plot of various concentrations of PQ (1-150 µM) (a-j) MoS_2-GNR modified GCE in 0.1 M PBS (pH 7.4)

5.3.4.5 Interference study

For the possible analytical application of the developed method in real samples, it is very crucial to determine the extent of interference on the voltammetric performance of MoS_2-GNR modified GCE towards PQ detection. The same was investigated by DPV in PBS of pH 7.4. Figure 5.12 demonstrates the interference effect on the modified electrode for the addition of 50 µM PQ in the co-existence of a 10-fold concentration of glucose, cholesterol, AA, L-cysteine, DA, creatine, glycine, oxalic acid, citrate, urea and UA in the form of a bar diagram. The obtained results indicate that the selected interfering species doesn't significantly affect the voltammetric response of PQ. So, the proposed sensor expresses an acceptable selectivity for PQ detection in the presence of

other coexisting species and hence it can be employed for PQ determination in real samples.

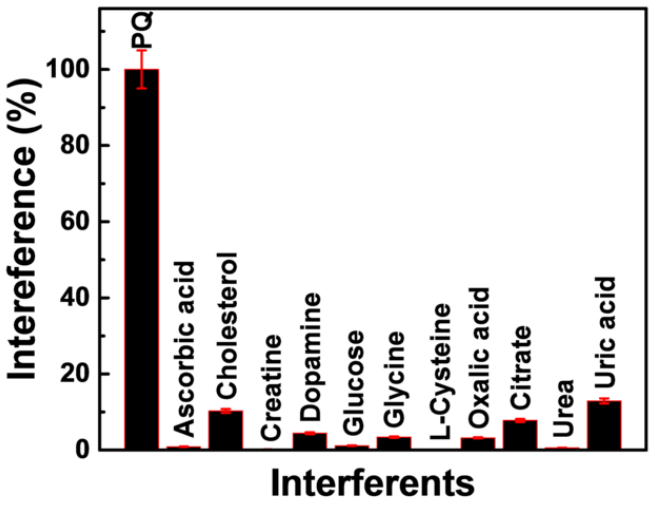

Figure 5.12 Interference study of potential interferents on the voltammetric response of 50 µM PQ. The interfering species concentration was 500 µM, and for PQ, it was 50 µM

5.3.4.6 Stability of the developed PQ sensor

The stability of a sensor is a very important parameter in assessing its overall sensing performance. The stability of the MoS_2-GNR/GCE was investigated for several hours in a single day at fixed intervals. The voltammetric signals were recorded for 50 µM PQ in 0.1 M PBS at RT. Figure 5.13 portrays the change in the current density for DPV response at different time intervals. It is clearly observed that the change in the oxidation current was less than 2 % after 8 hours indicating that the proposed sensor shows excellent stability for the quantitative estimation of PQ.

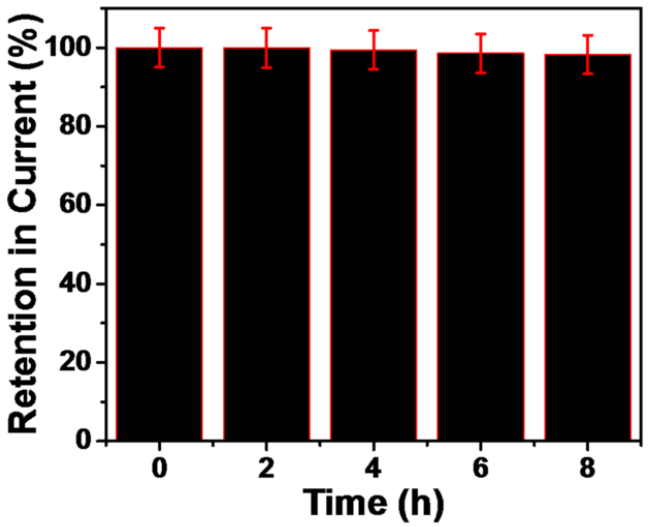

Figure 5.13 Intra-day stability examination of the developed electrochemical sensor by DPV in 0.1 M PBS at pH 7.4 with 50 μM PQ

5.3.4.7 Determination of PQ in human blood serum

The examination of the sensing performance of any drug sensor in human blood serum samples is very significant which determines its usefulness in practical applications such as in diagnostic centers. For this purpose, the human blood from a healthy human was collected and centrifuged to obtain a serum sample. The obtained serum sample was diluted ten times with PBS (pH 7.4) and the final pH of the resulting solution was checked to be 7.4 i.e. the physiological pH of the blood. DPV was applied to examine the sensing performance of the MoS_2-GNR modified GCE in serum samples. Firstly, the voltammogram was recorded in the blank test sample in the potential range from 0.3 V to 1.1 V and no oxidation/reduction peak was detected which indicates the non-existence of any redox-active compound in the chosen potential range. Then, the PQ solution was spiked step by step and the DPV response was recorded. It was observed that the current density of the anodic peak was escalated with each addition of PQ as displayed in Figure 5.14 (a). Figure 5.14 (b) shows the corresponding calibration plot

between the current density and concentration of PQ which expresses an approximately linear sensing behaviour in the concentration range from 3.98 µM to 117.65 µM. Figure 5.14 (b) inset illustrates that the calibration plot was obtained to be extremely linear in the concentration range of 3.98 - 64.89 µM. The LoD was calculated from the above-described formula. The value of LoD and sensitivity were calculated as 123.5 nM and 0.1804 $\mu A \mu M^{-1} cm^{-2}$ respectively.

Now, PQ detection was examined in the spiked blood serum samples and dilution was performed in a similar manner as described earlier. The standard addition method was employed for calculating the recovery of the proposed electrochemical sensor. The standard solutions of PQ were added to the serum solution under investigation and the above prepared calibration plot was exploited to estimate the amount of PQ present in the solution. The obtained results of the recovery calculation are presented in the Table 5.3

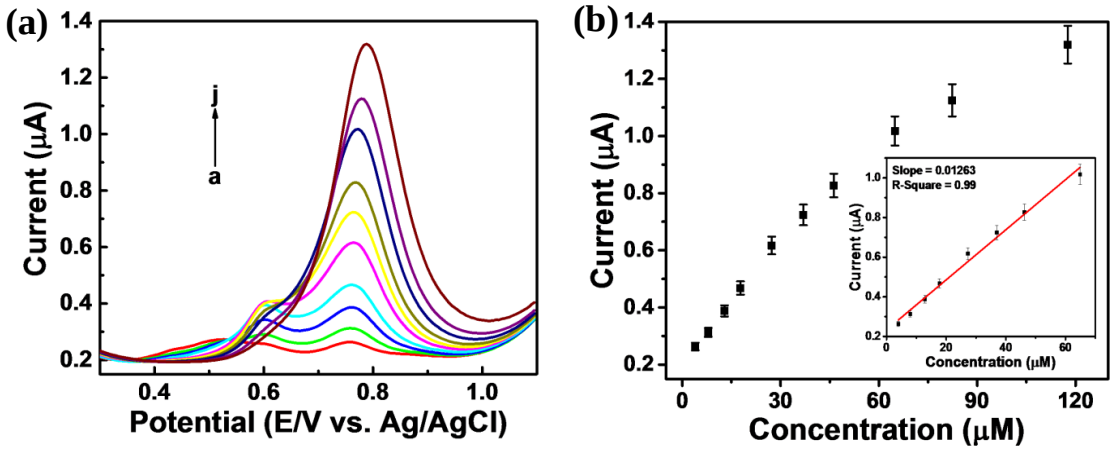

Figure 5.14 (a) DPV curves and (b) linear calibration plot of various concentrations of PQ (3.98-117.65 µM) (a-j) MoS_2-GNR modified GCE in human blood serum samples.

Table 5.3 DPV determination of PQ in spiked blood serum samples

S.N.	Actual amount of PQ (µM)	Calculated amount of PQ (µM)*	Recovery (%)
1	17.81	18.61	104.49
2	46.26	47.04	101.68
3	64.89	62.18	95.82

*Mean average of three estimations.

5.3.4.8 Detection of PQ in pharmaceutical preparations

The catalytic efficacy of the developed sensor for PQ was validated in the pharmaceutical preparations. The PQ tablet was used as a real sample for PQ detection and the tablet was obtained from a local drug store. The tablet was weighed and crushed properly followed by the addition of an ethanol-water mixture. The mixture was sonicated, filtered with Whatman filter paper, and centrifuged at 7000 rpm. The resulting filtrate was used to spike the test solution, and the amount of PQ was determined through DPV. The calibration plot already prepared was utilized, and the standard addition method was applied and the recovery calculations were carried out. Table 5.4 expresses the results of the recovery test. The result clearly signifies the importance of our developed sensor displaying a recovery of 97-110%. The work has also been compared to the previously reported methodologies on the ground of linear range and LoD, and displayed in Table 5.5. The table shows that our developed sensor based on MoS_2-GNR has better and more stable performance over the wide linear concentration range of PQ with better LoD.

Table 5.4 DPV determination of PQ in the tablet

S.N.	Actual amount of PQ (µM)	Calculated amount of PQ (µM)*	Recovery (%)
1	19.18	18.67	97.35
2	26.80	29.22	109.02
3	38.18	41.37	108.35
4	56.98	55.87	98.04

*Mean average of three estimations.

Table 5.5 Comparison of electrochemical sensing works of PQ reported in the literature

Summary of characteristics of analytical methods for PQ in different samples						
Modified Electrode	**Technique**	**Supporting electrolyte**	**LoD (µM)**	**Linear Range (µM)**	**Matrix**	**Reference**
Fullerene C60 monoadduct-MIP/PGE	DPASV	BR pH 7.5	0.0008	0.003-0.848	Human blood serum, urine & Pharmaceutical formulation	[Prasad et al., 2016]
AuNu/GCE	DPV SWV	PBS pH 5	0.0035 0.0009	0.01-1 0.001-1	Human blood serum & Pharmaceutical formulation	[Thapliyal et al., 2017]
Cu-NW-CPE	DPV	PBS pH 5.5	0.964	2.236-22.711	Pharmaceutical formulation	[Mashhadizadeh and Akbarian, 2009]
MWCNTs/GCE	SWV	BR and KCl pH 7	0.028	0.1-5	Urine	[Marlin et al., 2019]
PANI-Co_3O_4/GCE	DPV	PBS pH 3.5	0.002	20-36	Urine	[Nate et al., 2021]

GCE	LSV DPV SWV	BR pH 4	36.2 16.2 6.94	$30\text{-}10^4$ 30-100 30-100	Pharmaceutical formulation	[Arguelho et al., 2005]
MoS_2-GNR	DPV	PBS pH 7.4	-	-	Human blood serum & Pharmaceutical formulation	[Present work]

MIP=Molecularly imprinted polymer, AuNu= Gold nanourchins, Cu-NW=$Cu(OH_2)$ Nanowire, PGE= Pyrolytic graphite electrode , MWCNTs= Multi-walled carbon nanotubes , DPASV= Differential pulse anodic stripping voltammetry, BR=Borate buffer

5.4 Conclusion

A sensitive and selective sensor was successfully developed for the detection of PQ based on GNR and MoS_2 nanosheets. This nanostructured composite material showcased a high electrocatalytic activity towards the oxidation of PQ, characterized by an enhanced voltammetric current density at a physiological pH. The excellent sensitivity is accredited to the larger effective surface area and highly conductive behaviour of GNR. The voltammetric analyses have revealed that the developed sensor has a very low LoD value. It has immense potential for application in PQ detection in biological fluids and pharmaceutical formulations. Also, the proposed method can be used as a detection tool in diagnostic centers as well as can be appropriate for quality control units.